

# The XMM-LSS catalogue: X-ray sources and associated optical data. Version I

M. Pierre<sup>1\*</sup>, L. Chiappetti<sup>2</sup>, F. Pacaud<sup>1</sup>, A. Gueguen<sup>1</sup>, C. Libbrecht<sup>1</sup>,  
B. Altieri<sup>3</sup>, H. Aussel<sup>1</sup>, P. Gandhi<sup>4†</sup>, O. Garcet<sup>5</sup>, E. Gosset<sup>5</sup>, L. Paioro<sup>2</sup>, T.J. Ponman<sup>6</sup>,  
A.M. Read<sup>7</sup>, A. Refregier<sup>1</sup>, J.-L. Starck<sup>8,1</sup>, J. Surdej<sup>5</sup>, I. Valtchanov<sup>3</sup>,  
C. Adami<sup>9</sup>, D. Alloin<sup>1</sup>, A. Alshino<sup>6</sup>, S. Andreon<sup>10</sup>, M. Birkinshaw<sup>11</sup>, M. Bremer<sup>11</sup>, A. Detal<sup>5</sup>,  
P.-A. Duc<sup>1</sup>, G. Galaz<sup>12</sup>, L. Jones<sup>6</sup>, J.-P. Le Fèvre<sup>8</sup>, O. Le Fèvre<sup>9</sup>, D. Maccagni<sup>2</sup>, A. Mazure<sup>9</sup>,  
H. Quintana<sup>12</sup>, H. J. A. Röttgering<sup>13</sup>, P.-G. Sprimont<sup>5</sup>, C. Tasse<sup>13</sup>,  
G. Trinchieri<sup>2</sup>, J.P. Willis<sup>14</sup>

<sup>1</sup> Laboratoire AIM, CEA/DSM - CNRS - Université Paris Diderot, DAPNIA/Service d'Astrophysique, Bt. 709, CEA-Saclay, F-91191 Gif-sur-Yvette Cedex, France

<sup>2</sup> INAF, IASF Milano, via Bassini 15, I-20133 Milano, Italy

<sup>3</sup> ESA, Villafranca del Castillo, Spain

<sup>4</sup> Institute of Astronomy, Madingley Road, Cambridge CB3 0HA, UK

<sup>5</sup> Institut d'Astrophysique et de Géophysique, Université de Liège, Allée du 6 Août, 17, B5C, 4000 Sart Tilman, Belgium

<sup>6</sup> School of Physics and Astronomy, University of Birmingham, Edgbaston, Birmingham, B15 2TT, UK

<sup>7</sup> Department of Physics and Astronomy, University of Leicester, Leicester LE1 7RH, UK

<sup>8</sup> DAPNIA/SEDI CEA Saclay, 91191 Gif sur Yvette

<sup>9</sup> Laboratoire d'Astrophysique de Marseille, France

<sup>10</sup> INAF, Osservatorio Astronomico di Brera, Milan, Italy.

<sup>11</sup> Department of Physics, University of Bristol, Tyndall Avenue, Bristol BS8 1TL, UK.

<sup>12</sup> Departamento de Astronomía y Astrofísica, Pontificia Universidad Católica de Chile, Santiago, Chile.

<sup>13</sup> Leiden Observatory, P.O. Box 9513, 2300 RA Leiden, The Netherlands.

<sup>14</sup> Department of Physics and Astronomy, University of Victoria, Elliot Building, 3800 Finnerty Road, Victoria, BC, V8P 1A1 Canada.

## ABSTRACT

Following the presentation of the XMM-LSS X-ray source detection package by Pacaud et al., we provide the source lists for the first 5.5 surveyed square degrees. The catalogues pertain to the [0.5–2] and [2–10] keV bands and contain in total 3385 point-like or extended sources above a detection likelihood of 15 in either band. The agreement with deep logN–logS is excellent. The main parameters considered are position, countrate, source extent with associated likelihood values. A set of additional quantities such as astrometric corrections and fluxes are further calculated while errors on the position and countrate are deduced from simulations. We describe the construction of the band-merged catalogue allowing rapid sub-sample selection and easy cross-correlation with external multi-wavelength catalogues. A small optical CFHTLS multi-band subset of objects is associated with each source along with an X-ray/optical overlay. We make the full X-ray images available in FITS format. The data are available at CDS and, in a more extended form, at the Milan XMM-LSS database.

**Key words:** catalogues, surveys, X-rays: general

## 1 INTRODUCTION

The XMM Large Scale Structure Survey (XMM-LSS) has been designed to provide a well defined statistical sample of X-ray galaxy clusters out to a redshift of unity, over a single large area, suitable for cosmological studies (Pierre et al. 2004). This requires the

\* E-mail: mpierre@cea.fr

† Present address: RIKEN Cosmic Radiation Lab, 2-1 Hirosawa, Wakoshi, Saitama, 351-0198, Japan

ability to detect and characterize faint extended sources, in such a way as to control both the selection effects and the contamination by spurious or misclassified pointlike sources. For this purpose, we have developed a dedicated X-ray image processing package, XAMIN, which is adapted to the complex characteristics of the XMM focal plane (Pacaud et al. 2006). It is a two-step procedure combining wavelet multi-resolution analysis and maximum likelihood fits, both using Poisson statistics. The package has been extensively tested and its parameters adjusted by means of simulations, for the extended (clusters) and pointlike (AGN) source populations; the latter representing some 95% of the X-ray sources at our sensitivity of  $\sim 4 \cdot 10^{-15}$  erg s $^{-1}$  cm $^{-2}$  in the [0.5-2] keV band.

The first reports on cluster and AGN populations, based on the XAMIN products and associated selection function, were published by Pierre et al. (2006) and Gandhi et al. (2006) respectively.

The guaranteed time pointings (G fields in Table 1) were previously analysed with an independent, more traditional pipeline analogous to the one used for the HELLAS2XMM survey (Baldi et al. 2002), as described in Chiappetti et al. (2005), providing also the standard reference for the Milan XMM-LSS database.

The XMM-LSS survey, located around  $2^h 30^m -5$  deg is associated in the optical with the Wide Synoptic component of the Canada France Hawaii Telescope Legacy Survey<sup>1</sup> (CFHTLS - W1).

In this paper, we present the source lists obtained for the first 45 XMM-LSS pointings processed by XAMIN along with the relevant information on the catalogues (Sec. 2) as well as the X-ray images (Sec. 3.1). Sec. 3.2 describes the associated optical data that we make publicly available. The online facilities and plans for future releases are presented in the two last sections.

## 2 THE X-RAY SOURCE LISTS

### 2.1 List of available pointings

The XMM-LSS pointings pertaining to the Guaranteed Time, AO-1 and AO-2 periods are listed in Table 1 and displayed in Fig. 1. The raw X-ray observations (ODFs) were reduced using the standard XMM Science Analysis System (XMMSAS; version v6.1) tasks `emchain` and `epchain` for the MOS and pn detectors respectively. High background periods, related to soft protons, were excluded from the event lists following the procedure outlined by Pratt & Arnaud (2002). The resulting light curves were visually inspected. After this operation, a number of pointings appeared to be not usable for the purpose of the XMM-LSS survey (too low effective exposure times) and, consequently, are not included in the present version of the catalogue. The fields in question were re-observed during AO-5 (July 2006 - January 2007) and will be published in a subsequent data release.

### 2.2 Processing and XAMIN output source parameters

Photon images in different energy bands are then created with a scale of  $2''.5$  pixel $^{-1}$ . Images from the three detectors (pn, MOS1, MOS2), pertaining to the same band, are co-added. The resulting image is in turn filtered in wavelet space<sup>2</sup> to remove the noise at a given significance level and subsequently scanned by a source detection algorithm set to a low threshold to obtain a primary source

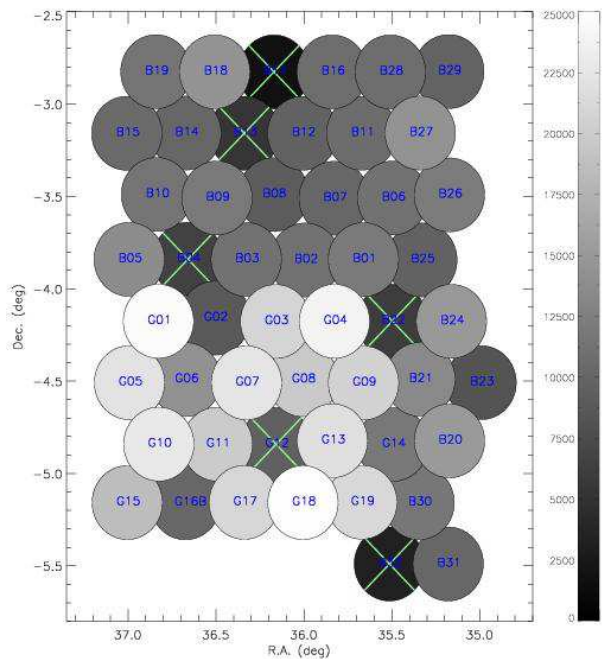


**Figure 1.** Lay-out of the Guaranteed Time, AO-1 and AO-2 pointings. The grey scale indicates the effective exposure times. Pointings not included in the present release (see Table 1) are flagged by a cross. The total resulting geometrical area, taking a radius of  $13'$  for the pointing useful radius (Sec. 2.3.1) amounts to  $5.5$  deg $^2$ .

list. Detailed properties of each detected source are further assessed from the individual photon images using XAMIN, a maximum likelihood profile fitting procedure<sup>3</sup> designed for the XMM-LSS survey. The specific goal of this second pass is to monitor in a clean and systematic way the characterization of extended X-ray sources and associated selection effects. The principle and performances of XAMIN, for extended and point-like sources, are described in detail by Pacaud et al. (2006) and we recall here the main lines of the procedure. Basically, for each source, two spatial emission models convolved by the XMM Point Spread Function (PSF) are tested: (pnt) a point source and (ext) a  $\beta$ -profile assuming a constant slope of  $2/3$ . The main parameters returned are the position and the fitted countrates and, for model `ext`, the best estimate of the core radius of the  $\beta$ -model. Further, for each model, the likelihood<sup>4</sup> of the source is computed, as well as the likelihood of the extension for model `ext`. The fits are simultaneously performed on the pn and on the MOS1+MOS2 sum images only requiring the source centre to be the same in both images<sup>5</sup>. The procedure takes into account all main technical characteristics such as: the blurring of the PSF and the vignetting as a function of off-axis angle and photon energy, the gaps between the CCD of the pn and MOS arrays, and the various background contributions. Results of the `ext` fit allow us to define two classes of extended objects in the XAMIN parameter space: the C1 and C2 classes (see Sec. 2.3.4). Table 2 summarises

<sup>3</sup> the likelihood is computed with respect to a flat image

<sup>4</sup> The values actually provided are the natural logarithm of the likelihoods but, to follow the widely spread usage, we shall call them simply “likelihood” throughout the paper. We refer to Pacaud et al. (2006, Sec. 2.3.1) for clarification of this terminology issue.

<sup>5</sup> In the case of model `ext`, an additional fitting condition imposes that the core radii inferred from the pn and MOS1+MOS2 images are the same

<sup>1</sup> <http://cfht.hawaii.edu/Science/CFHTLS/>

<sup>2</sup> à *trou* algorithm, combined with a Poisson noise model; see Starck & Pierre (1998)

**Table 1.** The individual XMM-LSS pointings. Quoted exposures are effective exposures computed after filtering high background periods; pointings with too low exposures (which have been re-executed during the XMM AO-5) are indicated by a star and are not included in the source list presented in this paper. Shifts are the astrometric corrections:  $\Delta RA/\cos(\text{Dec}) = RA_{XMM} - RA_{correct}$ ,  $\Delta Dec = Dec_{XMM} - Dec_{correct}$  (see Sec. 2.3.3); last column indicates whether the correction is based on CFHTLS W1 data (1), see Sec. 3, or on the USNO-A2 catalogue (2). The letter G refers to the Liège/Milan/Saclay Guaranteed Time (nominal exposure time: 20 ks) and the letter B to the observations performed during the Guest Observer phases (nominal exposure time: 10 ks).

Field id		RA (J2000)	Dec (J2000)	Exposure times (ks)			Astrometric correction		
Internal	XMM ID			MOS1	MOS2	pn	$\Delta RA$ (")	$\Delta Dec$ (")	Origin
G01	112680101	02:27:25.4	-04:11:06.4	24.6	25.3	21.4	-1.60	+0.53	1
G02	112680201	02:25:54.2	-04:09:05.6	10.1	9.7	6.7	-1.07	+0.00	1
G03	112680301	02:24:45.6	-04:11:00.8	21.8	21.7	17.3	-1.07	+1.07	1
G04	109520101	02:23:25.3	-04:11:07.6	25.5	25.8	19.5	-1.60	+0.53	1
G05	112680401	02:28:05.1	-04:31:08.1	23.5	23.9	12.5	-1.07	+1.07	1
G06	112681301	02:26:34.4	-04:29:00.8	16.4	16.6	10.5	-0.53	+0.53	1
G07	112681001	02:25:25.3	-04:31:07.1	22.5	25.1	18.6	-0.53	+0.00	1
G08	112680501	02:23:54.6	-04:29:00.1	21.2	21.3	15.9	+0.00	+1.07	1
G09	109520601	02:22:45.2	-04:31:11.1	22.5	22.7	16.4	+0.00	+0.53	1
G10	109520201	02:27:25.4	-04:51:04.4	24.7	24.6	18.5	-1.07	+1.07	1
G11	109520301	02:26:05.1	-04:51:06.1	21.7	21.8	16.1	-1.06	+0.53	1
G12*	109520401	02:24:45.4	-04:51:11.2	not used			-0.54	+0.53	1
G13	109520501	02:23:13.1	-04:49:03.1	23.6	23.9	17.8	-2.67	-0.53	1
G14	112680801	02:22:04.1	-04:51:09.7	14.4	14.1	8.3	+1.06	+0.53	1
G15	111110101	02:27:54.1	-05:09:02.3	20.8	21.8	14.0	-2.67	+0.00	1
G16a*	111110201	02:26:34.2	-05:09:03.1	not used			-1.60	+0.53	1
G16b	111110701	02:26:35.2	-05:08:46.6	11.9	11.9	11.5	+0.00	+0.53	1
G17	111110301	02:25:14.3	-05:09:08.4	22.4	22.2	17.5	-2.67	-0.53	1
G18	111110401	02:23:54.1	-05:09:09.7	27.7	28.0	19.2	-2.67	+0.00	1
G19	111110501	02:22:34.0	-05:09:02.1	23.2	23.8	16.8	-2.67	+0.00	1
B01	037980101	02:22:45.5	-03:50:58.8	14.1	14.2	8.3	-2.13	+0.00	1
B02	037980201	02:24:05.6	-03:51:00.0	13.2	13.2	7.8	-2.13	+0.00	1
B03	037980301	02:25:25.7	-03:50:59.2	13.3	13.0	7.9	-1.07	+0.53	1
B04*	037980401	02:26:45.4	-03:51:00.1	not used			-1.07	+0.53	1
B05	037980501	02:28:05.4	-03:51:00.5	15.7	15.7	10.5	-0.53	+1.06	1
B06	037980601	02:22:05.6	-03:31:00.2	13.2	13.2	7.7	-1.60	+0.53	2
B07	037980701	02:23:25.7	-03:30:56.7	12.3	12.3	6.9	-3.73	+0.00	2
B08	037980801	02:24:34.3	-03:29:05.1	10.6	11.5	6.3	-0.53	+1.07	2
B09	037980901	02:26:05.4	-03:31:01.1	13.9	13.8	8.9	-0.54	+0.53	2
B10	037981001	02:27:14.2	-03:28:58.7	13.0	13.2	8.6	-1.07	+2.13	2
B11	037981101	02:22:34.2	-03:09:02.5	12.4	12.3	7.9	-3.20	+1.07	2
B12	037981201	02:23:54.4	-03:09:04.1	11.4	11.3	7.0	-3.20	+0.00	2
B13*	037981301	02:25:14.4	-03:08:57.4	not used			-0.53	+1.60	2
B14	037981401	02:26:34.4	-03:08:57.6	12.6	12.5	6.6	-0.53	+3.73	2
B15	037981501	02:27:54.6	-03:08:59.3	11.4	11.5	8.4	-2.13	+1.07	2
B16	037981601	02:23:14.4	-02:48:56.3	12.3	12.7	7.9	-1.60	+2.13	2
B17*	037981701	02:24:34.8	-02:48:50.0	not used			-2.67	+3.73	2
B18	037981801	02:25:55.0	-02:48:49.1	16.0	16.2	11.4	-1.07	+2.13	2
B19	037981901	02:27:14.9	-02:48:49.5	13.1	13.1	8.7	-1.07	+2.13	2
B20	037982001	02:20:34.8	-04:48:46.3	16.1	16.8	11.7	-1.60	-0.53	1
B21	037982101	02:21:14.9	-04:28:45.9	15.6	15.6	9.9	-2.13	+0.53	1
B22*	037982201	02:22:05.5	-04:11:03.9	not used			+0.00	+0.00	1
B23	037982301	02:20:05.5	-04:31:03.9	9.0	9.6	6.5	-1.07	+1.60	1
B24	037982401	02:20:45.6	-04:11:01.2	18.1	18.2	10.4	-1.07	+0.53	1
B25	037982501	02:21:25.5	-03:51:02.4	11.5	11.9	6.8	-1.07	-0.53	1
B26	037982601	02:20:34.8	-03:28:50.4	14.7	14.6	8.3	-2.13	+0.53	2
B27	037982701	02:21:14.8	-03:08:49.1	16.3	16.2	10.7	-1.60	+1.07	2
B28	147110101	02:21:55.1	-02:49:02.4	11.4	11.6	9.1	-1.60	+0.00	2
B29	147110201	02:20:35.1	-02:49:00.1	10.6	10.6	8.2	-1.60	+0.00	2
B30	147111301	02:21:15.1	-05:09:00.7	12.4	12.5	9.9	-1.07	+0.53	1
B31	147111401	02:20:36.3	-05:28:59.5	10.8	11.0	8.4	-0.53	+0.53	1
B32*	147111501	02:21:56.0	-05:28:56.4	not used			-3.20	+0.53	1

**Table 2.** XAMIN output parameters (Pacaud et al. 2006).

See Pacaud et al. (2006) for the statistical definition of the derived likelihood values

Notes: <sup>a</sup> computed for both point-like and extended profile fits,

<sup>b</sup> issued for each of the three EPIC detectors.

Parameter	Notes	Content
CUTRAD		Size of the fitting box
EXP	b	Mean exposure time in the box
GAPFLAG	b	Distance to nearest CCD gap
GAP_NEIGHBOUR		Distance to nearest detected neighbour in the fitting box
EXT		Best fit core radius
EXT_LH		Extension likelihood
DET_LH	a	Detection likelihood
X_IMA, Y_IMA	a	Best fit position in pixel
RA, DEC	a	Best fit sky coordinates
RATE_MOS	a	EPIC-MOS count rate
RATE_PN	a	EPIC-pn count rate
SCTS_MOS	a	Estimated source counts in MOS1+2
SCTS_PN	a	Estimated source counts in pn
BG_MAP_MOS	a	Background level in MOS1+2
BG_MAP_PN	a	Background level in pn
PIX_DEV	a	Distance between input/output position
N_ITER	a	Number of iterations in the fit

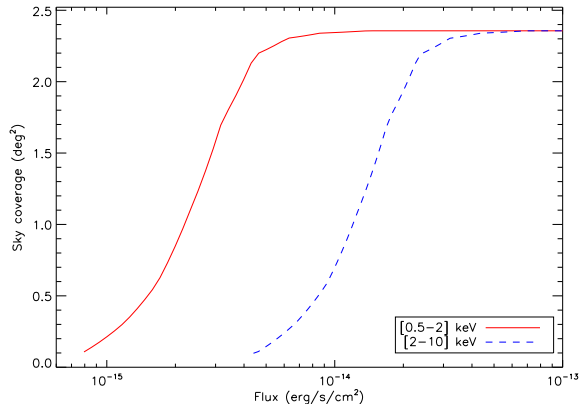
**Table 3.** Mean total background level (MOS1 + MS2 + pn) for the pointings included in the present catalogue, as a function of off-axis angle. Units are  $10^{-6}$  counts/s/pixel for a pixel size of  $2.5''$ 

Off-axis	[0.5-2] keV	[2-10] keV
0' - 5'	7.1	12.7
5' - 10'	6.3	12.4
10' - 13'	5.8	12.2

the output parameters of the pipeline. Table 3 provides the background level, averaged over all pointings included in the present catalogue. The measurements were performed on the X-ray images (obtained after removing bad time intervals) by masking the detected source regions, for three ranges of off-axis distance. We recall that the background consists of two components: (1) the cosmic background which is affected by the vignetting and (2) the particle background, which is significant at high energy and not affected by the vignetting. As a rule of thumb, a point-like source detected with 15 net photons in any of the 3 rings shows a signal to noise ratio of  $\sim 3.6$  and  $3.3$  for the [0.5-2] and [2-10] keV bands respectively (when considering a circular aperture having a radius of  $10''$ ).

### 2.3 Source list description

In this paper, we present the source lists for two bands, [0.5-2] and [2-10] keV, named B and CD respectively. Tables 9 and 10 display the parameters we make available: in addition to the XAMIN output, a number of parameters are a posteriori calculated in order to facilitate the interpretation of the data set. In its present state, XAMIN does not perform error calculations. Mean statistical errors were estimated by means of extensive simulations. Pacaud et al. (2006) presented a detailed account of uncertainty estimates for the extended sources (count rate and core radius). In the present paper, further error information is provided for the point source population; we note that only the first 2 digits are to be considered sig-

**Figure 2.** Sky coverage for the [0.5-2] and [2-10] keV bands corresponding to 27 pointings of 10 ks. The curve in the soft band is derived from extensive simulations of point sources and includes only sources having a detection likelihood  $> 15$  within off-axis distances less than  $10'$ . The hard curve is scaled from the soft one on the basis of equivalent signal to noise ratio, using adequate background, vignetting and PSF characteristics.

nificant for the count rate and for the core radius as well as for the derived quantities.

#### 2.3.1 Thresholds

XAMIN processes sources only out to an off-axis distance of  $13'$  by applying a detection mask centred on the mean optical axis of the 3 telescopes, considering in this way only sources that are visible by the 3 detectors. The total geometrical area of the present catalogue corresponding to the validated pointings indicated on Fig. 1 amounts to  $5.5 \text{ deg}^2$ . The present version of the B and CD band catalogues contains the extended sources identified as C1 and C2 (see Sec. 2.3.4) to which are added sources having a point source detection likelihood ( $LH$ ) greater than 15 (so-called *non-spurious*). As shown in Fig. 2, this ensures a 90% completeness limit of  $4 \times 10^{-15} \text{ erg s}^{-1} \text{ cm}^{-2}$  in the B band within an off-axis distance of  $10'$  for the 10ks pointings (beyond  $10'$ , the sensitivity falls below 50% of the value at the centre); in average, this corresponds to 85 and 70 sources per 20 ks and 10 ks pointing respectively, judged to be real within the inner  $13'$ .

#### 2.3.2 Count rate and Flux

XAMIN fits the MOS and pn count-rates independently<sup>6</sup> (assuming that the two MOS have the same response). We performed a number of point source tests by simulating a set of 30 images in which the logN-logS distribution was injected. We display in Fig. 3 the full range of simulations detailing the photometric accuracy out to an off-axis distance of  $13'$  (Pacaud et al. 2006, presented averaged performances). The Eddington bias is obvious for faint sources and increases with the off-axis distance; in particular the photometry appears to be unreliable for a number of sources detected with a total count-rate (pn+MOS1+MOS2) between 0.002 and 0.005 count/s at off-axis angle  $10' - 13'$ . These sources are however detected with a likelihood greater than 15, indicating that they are real. They are

<sup>6</sup> while the source position and extent are fixed to be the same for the 3 detectors

**Table 4.** Mean photometric bias ( $b$ ) and  $1\sigma$  error ( $e$ ), as a function of count-rate and off-axis distance for point sources, for each of the B and CD bands. Values (in percentile) are derived from 10 ks simulations considering sources having a detection likelihood  $> 15$  (cf Fig. 3); below count-rates of 0.003, the output locus is degenerate and the bias is too large to estimate meaningful errors. In order to lower the flux at which the bias arises, only sources having  $\text{gap}^* > 12''$  (cf Table 9) are used for the error calculation. The true count-rate is related to the observed quantity by:  $CR = CR_{obs}(100/(b + 100) \pm e/100)$

Band	B	CD
Countrate (count/s)	b, e	b, e
0 <off-axis< 5'		
0.003 < CR < 0.005	9, 21	9, 22
0.005 < CR < 0.0075	7, 15	8, 16
0.007 < CR < 0.01	6, 12	6, 12
0.01 < CR < 0.02	4, 8	4, 8
CR > 0.02	1, 4	1, 4
5 <off-axis< 10'		
0.003 < CR < 0.005	10, 26	11, 30
0.005 < CR < 0.0075	9, 19	9, 21
0.007 < CR < 0.01	7, 15	5, 11
0.01 < CR < 0.02	5, 10	2, 5
CR > 0.02	2, 5	1, 3
10 <off-axis< 13'		
0.003 < CR < 0.005	-	-
0.005 < CR < 0.0075	10, 24	11, 29
0.007 < CR < 0.01	9, 19	9, 21
0.01 < CR < 0.02	6, 13	7, 14
CR > 0.02	3, 7	3, 7

**Table 5.** The Energy Conversion Factors for the individual EPIC cameras and energy bands, stated in units of  $10^{-12} \text{ erg s}^{-1} \text{ cm}^{-2}$  for a rate of one count/s. A photon-index power-law of 1.7 and a mean  $N_H$  value of  $2.6 \cdot 10^{20} \text{ cm}^{-2}$  are supposed. The two MOS cameras are assumed to be identical.

Detector	B band	CD band
MOS	5.0	23
pn	1.5	7.9

thus left in the public source catalogue but their photometry should be handled with caution. Mean values for the photometric bias and accuracy are summarized in table 4.

Count-rate values are in turn converted into fluxes assuming a standard power law spectrum (photon index of 1.7) and the mean  $N_H$  value of the region ( $2.6 \cdot 10^{20} \text{ cm}^{-2}$ ). The Energy Conversion Factors are given in Table 5. The observed logN-logS distributions are presented in Fig. 4; they are in good agreement with the Vikhlinin et al. (1995) (ROSAT), Moretti et al. (2003) (ROSAT, Chandra and XMM), Baldi et al. (2002) (XMM) and Giommi et al. (2000) (BeppoSAX) data points.

Note that the resulting pn and MOS fluxes may be quite different for some sources. In most of the cases this is due to the fact that part of the source is occulted by a CCD gap in one of the detectors to the point where the information is not recoverable. Such cases can be identified from the gap-related columns (Tables 2 and 9) and it is suggested to use the fitted parameters obtained from the detectors on which the source is not affected by a gap (if any). For the sake of simplicity, a single mean flux

**Table 6.** Positional accuracy ( $1\sigma$  error on R.A. or Dec.) for point sources derived from simulations of 10 ks pointings and having a detection likelihood  $> 15$  (Fig. 5). Values are given for the B and CD bands, as a function of the summed measured count-rate:  $CR = \text{MOS1} + \text{MOS2} + \text{pn}$ . No selection is applied on the  $\text{gap}^*$  parameters (cf Table 9) but a  $3\sigma$  rejection is performed in the calculation of the errors. Because of the strong Eddington bias for faint sources located beyond  $R > 10'$  (Fig. 3), no positional errors are provided for output CR below 0.002 count/s.

Band	B	CD
Countrate (count/s)	Error (")	Error (")
0 <off-axis< 5'		
0.001 < CR < 0.002	2.0	2.0
0.002 < CR < 0.005	1.7	1.7
0.005 < CR < 0.01	1.3	1.3
CR > 0.01	0.8	0.8
5' <off-axis< 10'		
0.001 < CR < 0.002	2.0	2.0
0.002 < CR < 0.005	1.8	1.9
0.005 < CR < 0.01	1.5	1.5
CR > 0.01	1.0	1.0
10' <off-axis< 13'		
0.001 < CR < 0.002	-	-
0.002 < CR < 0.005	1.9	2.0
0.005 < CR < 0.01	1.6	1.7
CR > 0.01	1.2	1.3

value is provided ( $(\text{FLUX}(\text{MOS}) + \text{FLUX}(\text{pn}))/2$ )<sup>7</sup> along with column `fluxflag` indicating the difference between the fluxes inferred from the MOS1+MOS2 combination and the pn (0: less than 20%; 1: between 20-50%; 2: greater than 50%). For the two single-band catalogues, the sources are roughly equally distributed between the three categories of flux quality. Fluxes assuming a thermal spectrum as well as temperature and luminosity information for the extended sources classified as C1 and C2, confirmed as clusters, can be found in the XMM-LSS cluster database<sup>8</sup>.

### 2.3.3 Positional accuracy and astrometric corrections

The positional accuracy for the point source population was also estimated from the simulations. Results are displayed in Fig. 5 and summarised in Table 6. We recall here that for the point-like fit, as explained by Picaud et al. (2006), positions are fixed to those of the first pass catalogue (SExtractor detections on the wavelet filtered image).

In parallel, in order to compensate for possible inaccuracies in the XMM pointing positions, a global rigid astrometric correction was estimated using the SAS task `EPOSCORR`. We generated, for each XMM pointing, a reference X-ray list with all “non spurious” point-like sources along with a reference optical list containing all CFHTLS W1 objects within  $6''$  of the X-ray objects, being brighter than  $i' = 25$  and having a “good” or “fair” chance probability  $p < 0.03$  as defined in Sec. 3.3 (in the case where an X-ray source had more than one optical counterpart candidates, we retained only the one with the smallest chance probability). For

<sup>7</sup> as the MOS countrate is about 1/3 of the pn countrate for cluster spectra, the averaged MOS flux involves a number of photons comparable to that of the pn, thus justifying the simple mean

<sup>8</sup> <http://l3sdb.in2p3.fr:8080/l3sdb/>

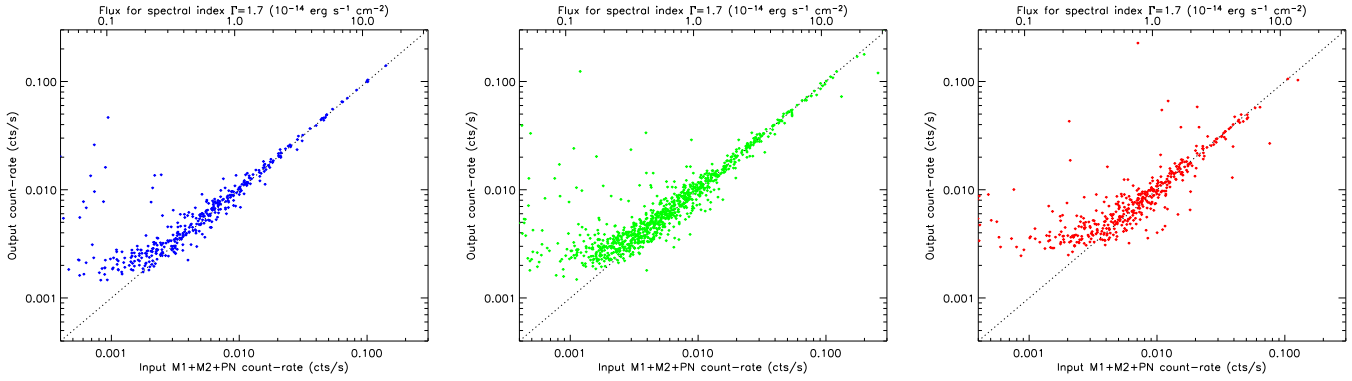


**Figure 3.** Photometric accuracy for three ranges of off-axis values from 10 ks simulated images in the soft band:  $0' - 5'$ ,  $5' - 10'$ ,  $10' - 13'$ . “Count-rate” is the measured MOS1+MOS2+pn rate, normalised to the on-axis value.

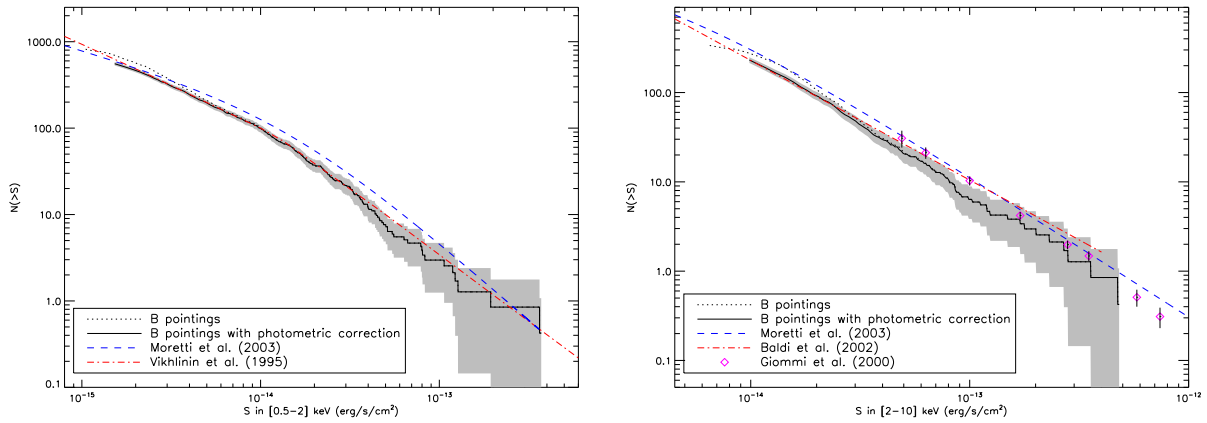


**Figure 4.** The logN-logS distributions for the soft (left) and hard(right) bands, involving the 27 pointings with  $\sim 10$  ks. Only sources having a detection likelihood  $> 15$  and an off-axis distance less than  $10'$  are considered. The dotted line corresponds to the raw counts and the solid line is corrected for the Eddington bias (as conspicuous in Fig. 7 of Pacaud et al. 2006). The dashed region indicates the  $1\sigma$  fluctuation level.

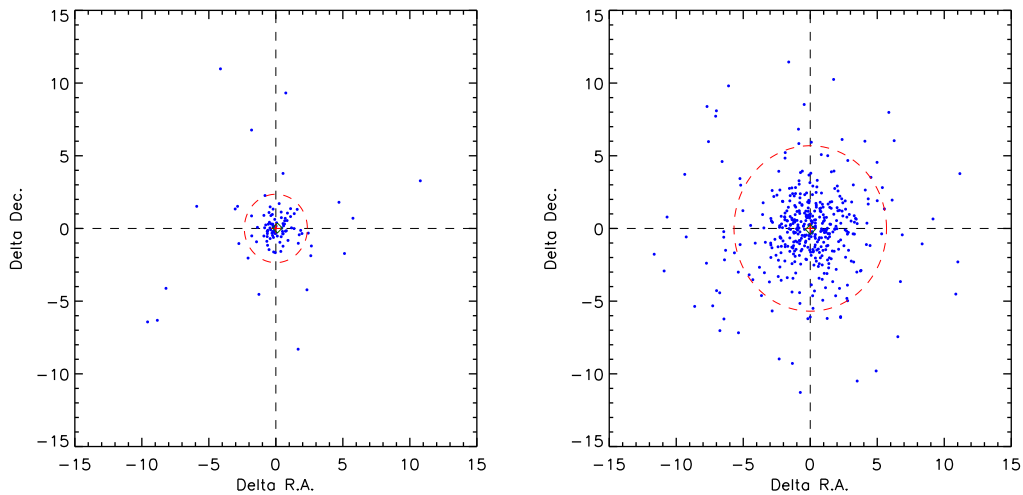


**Figure 5.** Example of positional accuracy diagrams resulting from the logN-logS point-source simulations of 10 ks exposures in the soft band. Left panel: *input - output* positions for the  $0 < \text{off-axis angle} < 5'$  and  $CR > 0.01$  sources; Right panel: *input - output* positions for the  $5' < \text{off-axis angle} < 10'$  and  $0.002 < CR < 0.005$  sources, where  $CR$  is the measured MOS1+MOS2+pn count-rate, normalised to the on-axis value. Axes are in unit of arcsec. The circle indicates the  $3\sigma$  rejection radius used to compute the mean positional error.

the three topmost rows of XMM pointings in Fig. 1, for which the CFHTLS data were not yet processed, the optical list was made from the USNO-A2 catalogue. The reference files were fed into EPOSCORR using the parameter `maxsig=2` to force removal of spurious matches. The offsets computed by EPOSCORR are plotted in Fig. 7. Offsets computed using USNO-A2 and CFHTLS objects are usually compatible within errors (with the nominal EPOSCORR errors being larger in the USNO-A2 case). The offsets given in Table 1 were applied to all coordinate sets for each source in the database. The database column `Xastrocorr` indicates whether the origin of the astrometric correction is the CFHTLS W1 or the USNO-A2 catalogue. Astrometrically corrected positions are used in the subsequent operations: removal of the redundant sources, source naming and cross-identification with the optical catalogue. Simulations of pairs of point sources separated by  $20''$  show that 67% of the pairs are resolved for sources having 30 photons each; all pairs being resolved when the sources contain 500 photons. As shown by Pacaud et al. (2006), a detection likelihood threshold of 15 eliminates almost all spurious detections (the corresponding contamination level is  $\sim 1\%$ ).

### 2.3.4 Extended source classification

Pacaud et al. (2006) and Pierre et al. (2006) presented in detail the criteria for defining galaxy cluster candidates. The selection is performed in the XAMIN output parameter space obtained in the soft band. This band presents the highest signal to noise ratio (S/N) at any redshift for typical cluster spectra (as well as for galaxy thermal halos) thus ensuring the highest completeness level for the extended source detection. The cluster candidate sample consists of two classes:

- The C1 class is defined such that no point sources are misclassified as extended and is described by `extent > 5''`, `likelihood of extent > 33` and `likelihood of detection9 > 32`. Note that while the C1 class is meant to be uncontaminated in terms of point-like sources, it contains a few nearby galaxies whose X-ray emission is unambiguously extended (Pacaud et al. submitted).

- The C2 class is described by `extent > 5''` and `15 < likelihood of extent < 33` (no condition on the `likelihood of detection`) and typically displays a contamination rate of 50%.

There are 73 C1 & C2 objects flagged in the catalogue, column `Bc1c2`. Note that, for the unique purpose of band merging (see below), a similar classification has been applied in the hard band. In this band, there are only 21 sources flagged as C2 and 1 flagged as C1, which are not detected in the soft one. Subsequent X-ray/optical inspection of these latter sources does not reveal, as expected, any new cluster. They are mostly weak sources at extreme off-axis angle, or unresolved doubles, or cluster X-ray centroids displaced by more than  $6''$  from the soft band position.

### 2.3.5 Band merging

Because X-ray colours serve as a useful piece of information for numerous science studies, we provide, in addition to the individual catalogues, the two-band merged catalogue. Band merging is a delicate operation given the rather large XMM PSF (FWHM  $\sim 6''$  at 1 keV on axis) and its variation with energy and off-axis distance.

It may also happen that a close pair is resolved in one band only, because of too low a photon number in the other band. In order to provide the community with an efficient and reliable tool, the construction of the merged catalogue received special attention and is described below.

As an X-ray source can be detected in one or two bands and, for each band, is independently fitted by the extended and point source models with the coordinates free, we adopt the following merging procedure. For each band, a source is classified as extended (E) if it satisfies `extent > 5''` and `likelihood of extent > 15` (i.e. C1 or C2 class); if not, it is classified as point-like (P). Then, pointing per pointing, we flag associations between the 2 bands within a search radius of  $6''$ . Note that we allow associations involving spurious sources ( $LH < 15$ ) at most in one band. We kept the information (rate, flux, etc.) about entries below this threshold in the merged catalogue, since it could be more useful (e.g. for upper limits) than no information at all, but we flag those cases with `Bspurious=1` or `CDspurious=1`. Finally, for each soft-hard couple in the merged catalogue, we define the **best band**, i.e. the band in which the detection likelihood of the source is the highest and from which the coordinates are taken. Details of the merging process are summarised in Table 7.

Starting from 2980 non-spurious sources in the soft band and 1255 non-spurious sources in the hard band, the resulting merged catalogue contains 3385 sources: out of them 50.5% are detected as point-like in the soft band only, 36.3% as point-like in both bands, 10.2% as point-like in the hard band only; 2.1% are candidate clusters of galaxies (soft band only). The remaining 0.8% are mostly borderline cases (cf end of Sec. 2.3.4). We note that in an extremely limited number of cases (4 couples of entries) the merging process gives ambiguous results, i.e. a detection in one band can be associated with two different detections in the other band. The flagging and naming of such cases is described in Sec. 2.3.7.

For *all* entries we provide in the database the distance between the positions found by XAMIN in the two energy bands (which in most cases could be used to solve the above ambiguities). Such an inter-band distance, for all the cases present in both bands, except for the few ambiguities, is within  $2''$  in 35% of the cases, within  $4''$  in 79% and above  $5''$  only in 9%. These percentages change to 39%, 83% and 7% if we exclude detections flagged as spurious in one band. If we compare the inter-band distance with the combination of the position errors computed according to the prescription in Table 6, we have that in 64% of the cases the inter-band distance is less than the  $1\sigma$  error, in 1.4% of the cases is above  $2\sigma$ .

### 2.3.6 Removal of redundant sources

Finally, in the case of redundant objects detected in the regions where the pointings overlap, we keep in the catalogues only the detection pertaining to the pointing where the source is the closest to the optical centre (cf columns `Boffaxis`, `CDoFFaxis` in Table 9). Except for a few ambiguous cases described in Section 2.3.7, a value of  $6''$  is found to be the adequate search radius to identify redundant detections. In this way, 280 doublets and a few triplets were identified and reduced to a single source.

### 2.3.7 Source naming

Objects in the merged catalogue are labelled following the IAU-style convention, i.e. `XLSS Jhhmmss.s-ddmmss`. The coordinates used in assigning the name are the ones deduced after the rigid

<sup>9</sup> for the ext fit

**Table 7.** Merging decisions and definition of the *best band*.

A source is defined as extended (E) in a given band if it satisfies  $\text{extent} > 5''$  and  $\text{likelihood of extent} > 15$  in this band. Otherwise it is defined as point-like (P).

For all sources, but the C1 clusters of galaxies, *flux* is computed from the ECF factors given in Table 5 using the point source rates.

For the C1 clusters, the fluxes are set to -1 as the reader is addressed to the XMM-LSS cluster database (spatial and spectral fitting providing accurate flux and luminosity measurements)

The numbers in [] indicate the number of spurious sources encountered in the inter-band associations (the counterpart in and B or CD is flagged as spurious i.e. has  $LH < 15$ )

B band	CD band	best band	Coordinates from	Flux in B	Flux in CD	# of sources
E	undetected	B	B E_fit	-1 for C1, <i>flux</i> for C2	-1	59
P	undetected	B	B P_fit	<i>flux</i>	-1	1710
undetected	E	CD	CD E_fit	-1	<i>flux</i>	22
undetected	P	CD	CD P_fit	-1	<i>flux</i>	347
E	E	where $\text{detlik\_ext}$ is max	best band E_fit	-1 for C1, <i>flux</i> for C2	-1 for C1, <i>flux</i> for C2	2
E	P	where $\text{detlik\_ext}$ is max	best band E_fit	-1 for C1, <i>flux</i> for C2	-1 for C1, <i>flux</i> for C2	12 [4 CD]
P	E	where $\text{detlik\_pnt}$ is max	best band P_fit	<i>flux</i>	<i>flux</i>	5
P	P	where $\text{detlik\_pnt}$ is max	best band P_fit	<i>flux</i>	<i>flux</i>	1228 [36 B, 358 CD]

astrometric correction, and chosen as official, i.e. those for the *best band* (see Table 7).

In the individual band catalogues, the sources are assigned supplementary names, following the same standard - XLSSx JHHMSS.S-DDMMSS - where x is B or CD and stands for the B and CD bands respectively. In this case, the coordinates correspond to the extended (E) or point-like (P) fit in the relevant band (Table 7). As a consequence of the merging procedure (Sec.2.3.5), the XLSS coordinate designation will coincide with one of the XLSSB or XLSSCD (i.e. for the *best band*).

In a limited number of cases (8 entries), a source in a band happens to be associated with two different objects in the other band. These couples of catalogue entries are flagged by a non-zero value in column *Xlink*, the registered value being a pointer to the other “ambiguous” entry in the couple. For those cases, the ambiguity in the XLSS name is resolved (when necessary, i.e. in 6 out of 8 cases) by the addition of a suffix : the two members of a couple will appear as XLSS JHHMSS.S-DDMSSa and XLSS JHHMSS.S-DDMSSb.

### 3 ASSOCIATED DATA PRODUCTS

#### 3.1 X-ray images

For each pointing, we make available - via the XMM-LSS database in Milan- the following images in FITS format. They are accessible as “data products” : for every source in the catalogue, a clickable link points to the images of the relevant pointings.

- The B and CD band photon images for the 3 detectors (after the event filtering).

- Exposure maps for the 3 detectors and the 2 bands. All images have a pixel size of  $2.5''$ . Note that the World Coordinate System (WCS) of the X-ray images is the one generated by the SAS, therefore it does not take into account the astrometric correction described in section 2.3.3 and quoted in Table 1. Consequently when overlaying X-ray source positions exactly on the X-ray images, one should use the coordinates labelled as “raw” in Table 9, although this does not make much difference for most of the sources, given the pixel size.

#### 3.2 Optical data

For each X-ray source of the merged catalogue, we provide:

- (i) the list of optical objects within a radius of  $6''$  around each X-ray source, extracted from the CFHTLS catalogue<sup>10</sup>. These data are available in the XMM-LSS database in Milan only, through the XLSSOPT table. Queries on X-ray lists are allowed and return the  $u^*, g', r', i', z'$  magnitudes and further optical information derived from the Terapix merged panchromatic catalogues.

- (ii) CFHTLS postage stamp images  $40'' \times 40''$  in the *i* and *g* bands (PNG format); in the case where a CFHTLS image is not yet processed, we provide a low exposure CFH12K image when available. An example is shown on Fig 6.

#### 3.3 A few statistics

Out of our 3385 X-ray sources, 2208 have at least one optical candidate closer than  $6''$ , 1071 fall in the area without CFHTLS coverage<sup>11</sup> (corresponding to the topmost three rows of XMM pointings in Fig. 1), while 106 have no optical association. The total number of associated optical objects is 6275 (the radius used here is 6 arc-sec irrespective of the fact the object is extended or point-like). A total of 472 X-ray sources have a single candidate within  $6''$ , 613 have two and the rest has more. The number of optical counterparts brighter than  $i' = 22.5$  is 1990 of which 55%, 36%, 14% are closer than respectively  $3'', 2'', 1''$  to an X-ray source (detected in any band). If we consider only the soft (B) band sources the numbers are 1826, 56%, 37%, 14% respectively, while for hard (CD) band sources they are 1094, 59%, 40%, 17%.

We further provide the distance  $d$  between the X-ray and optical positions as well as an estimate of the probability of chance coincidence

$$p = 1 - \exp(-\pi n(< m) d^2)$$

where  $n(< m)$  is the sky density of optical objects having an  $i'$  magnitude brighter than the magnitude  $m$  of the candidate counterpart, computed from the full CFHTLS W1 catalogue. Defining as “good” or “fair”, respectively, the X-ray/optical matches having  $p < 0.01$  and  $0.01 < p < 0.03$  (as described by Chiappetti et al. (2005)), we find 945 good associations and 637 fair ones. All the optical objects brighter than  $i' = 22.5$  and within  $1''$  and 87% of

<sup>10</sup> currently, from the T0003 W1 field release by Terapix: <http://terapix.iap.fr/>

<sup>11</sup> observed, but currently still under processing



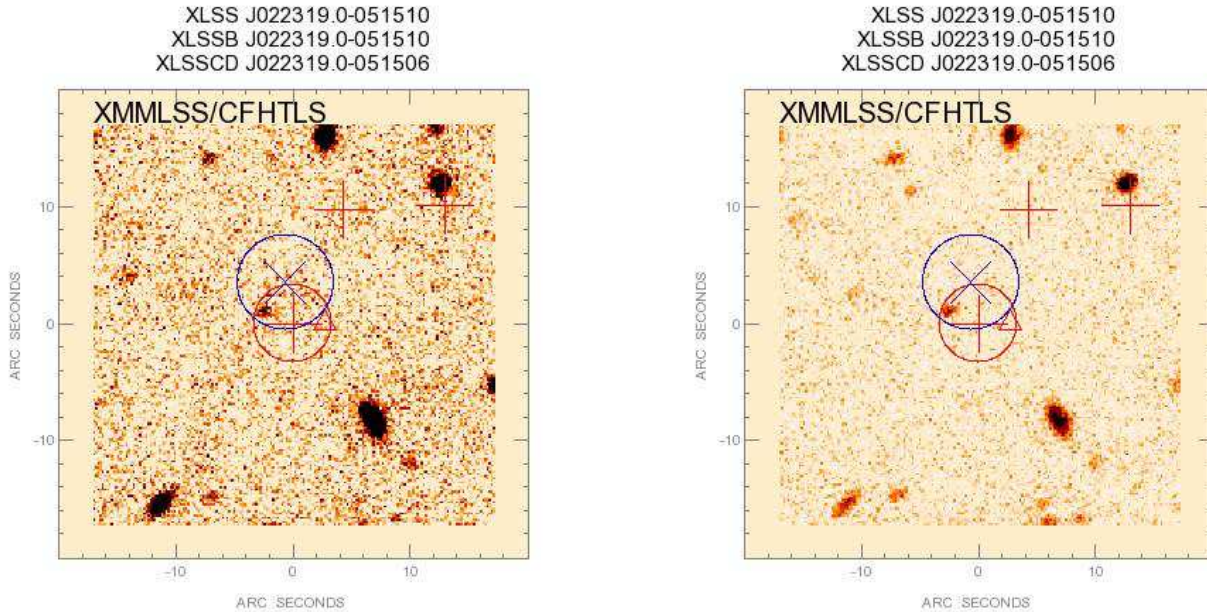


**Figure 6.** An example of postage stamp image centred on source XLSS J022319.0-051510. The CFHT *i* and *g*  $40'' \times 40''$  images are shown in left and right panels respectively. Soft sources are indicated by a red +, and hard ones by a blue x; all with astrometrically corrected positions. The original uncorrected position of the central source in the *best band* is indicated with a triangle of the corresponding color. The  $2\sigma$  radius mean error circles are indicated for the central source according to the values of Table 6. All sources within the  $40'' \times 40''$  field having  $LH > 15$  are plotted. North is up and East is left.

those within  $2''$  have a good probability, while for a distance within  $3''$  the percentage lowers to 69% for soft sources and 73% for hard sources.

#### 4 SUMMARY OF ONLINE AVAILABILITY

Online data access is summarised in Table 8. Namely, we provide :

- The raw XAMIN results in individual catalogues for the B [0.5-2] keV and CD [2-10] keV bands. Only sources above a detection likelihood of 15 are made available. Redundant sources detected in overlapping regions of different pointings are removed; data from the pointing where each object has the smallest off-axis angle are retained in the catalogue. In addition, fluxes assuming a power law spectrum are provided for each point-like source.
- The B-CD band merged catalogue assuming a correlation radius of  $6''$ . This required the definition of the *best band* from which a number of parameters, such as the position, are taken and, hence, a selection of information from the single band catalogues. Source counterparts in the other band are made available even if they have a detection likelihood below 15.
- Optical: panchromatic CFHTLS catalogue within  $6''$  of each source of the merged catalogue as well as *i'* and *g'* band  $40'' \times 40''$  png images.

The *main* parameters (listed in Tables 9 and 10) of the merged X-ray catalogue are available in electronic form at the Centre de Données de Strasbourg (CDS). The single-band and band-merged catalogues with *all* columns, as well as the associated data products (X-ray images and optical information) are accessible, with fully interactive selection, through the XMM-LSS database located in Milan and described by Chiappetti et al. (2005). User login details can be found in the entry web page.

#### 5 FUTURE

From now on, the XMM-LSS catalogue and associated data sets will be regularly incremented following the receipt of new XMM and CFHTLS pointings. In parallel, XAMIN is being upgraded with the inclusion of information on the photon energy for the source characterization, in such a way as to better discriminate between AGN and cluster sources. When the new version is validated, we foresee reprocessing the entire data set and making it publicly available with the corresponding documentation.

#### ACKNOWLEDGMENTS

The results presented here are based on observations obtained with XMM-Newton, an ESA science mission with instruments and contributions directly funded by ESA Member States and NASA. The cluster optical images were obtained with MegaPrime/MegaCam, a joint project of CFHT and CEA/DAPNIA, at the Canada-France-Hawaii Telescope (CFHT) which is operated by the National Research Council (NRC) of Canada, the Institut National des Sciences de l'Univers of the Centre National de la Recherche Scientifique (CNRS) of France, and the University of Hawaii. This work is based in part on data products produced at TERAPIX and the Canadian Astronomy Data Centre as part of the Canada-France-Hawaii Telescope Legacy Survey, a collaborative project of NRC and CNRS. AG acknowledges support from Centre National d'Etudes Spatiales. The Italian members of the team acknowledge financial contribution from contract ASI-INAF I/023/05/0. AD, OG, EG, PGS and JS acknowledge support from the ESA PRODEX Programme "XMM-LSS", and from the Belgian Federal Science Policy Office for their support. HQ acknowledges partial support

**Table 8.** The XMM-LSS X-ray and optical data products. Individual parameter availability is given in Tables 9 and 10

Data sets		Location	Address
Merged XLSS catalogue, main parameters		CDS	<a href="http://cdsweb.u-strasbg.fr/cgi-bin/qcat?J/MNRAS/vol/pag">http://cdsweb.u-strasbg.fr/cgi-bin/qcat?J/MNRAS/vol/pag</a>
Single-band catalogues:	XLSSB, XLSSCD	Milan	<a href="http://cosmos.iasf-milano.inaf.it/~lssadmin/Website/LSS/Query">http://cosmos.iasf-milano.inaf.it/~lssadmin/Website/LSS/Query</a>
Merged catalogue (all parameters):	XLSS		
X-ray images			
Optical catalogue :	XLSSOPT		
Optical postage stamps			

from the FONDAP Centro de Astrofisica. PG is a Fellow of the Japan Society for the Promotion of Science.

## REFERENCES

- Baldi A., Molendi S., Comastri A., Fiore F., Matt G., Vignali C., 2002, *ApJ*, 564, 190  
 Chiappetti L. et al., 2005, *A&A*, 439, 413  
 Gandhi P. et al., 2006, *A&A*, 457, 393  
 Giommi P., Perri M., Fiore F., 2000, *A&A*, 362, 799  
 Moretti A., Campana S., Lazzati D., Tagliaferri G., 2003, *ApJ*, 588, 696  
 Pacaud F. et al., 2006, *MNRAS*, 372, 578  
 Pierre M. et al., 2006, *MNRAS*, 372, 591  
 Pierre M. et al., 2004, *Journal of Cosmology and Astro-Particle Physics*, 9, 11  
 Pratt G. W., Arnaud M., 2002, *A&A*, 394, 375  
 Starck J.-L., Pierre M., 1998, *A&AS*, 128, 397  
 Vikhlinin A., Forman W., Jones C., Murray S., 1995, *ApJ*, 451, 553

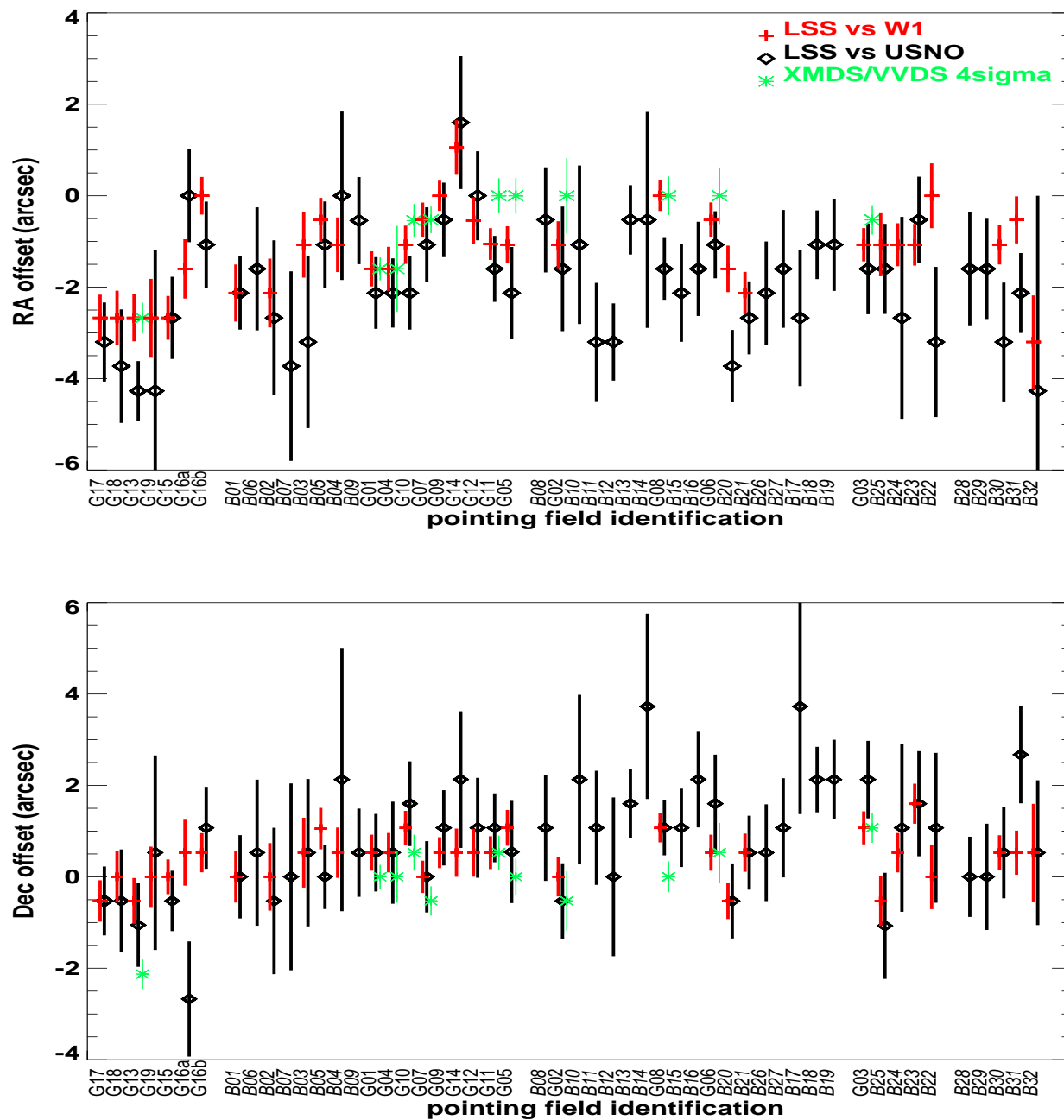


**Figure 7.** Astrometric correction offsets in RA (top panel) and Dec (bottom panel), with nominal error bars computed by EPOSCORR. Diamonds indicate the offsets computed using the USNO-A2 catalogue, crosses those using CFHTLS W1 data, and asterisks the offsets used in Chiappetti et al. (2005), when applicable. Different offsets for the same field are displaced horizontally for clarity. The x-axis gives the XMM pointings in chronological order of execution, with different observation "seasons" separated by a blank space.

**Table 9.** List of parameters provided in the public XMM-LSS catalogue. All are available at the XMM-LSS Milan database in separate tables XLSSB for the soft band and XLSSCD for the hard band (the column name has an appropriate prefix : when there are two column names given, one with the prefix B and one with the prefix CD, only the one applicable to the given band appears in the relevant table but both may show up in the band-merged table; column names without prefix are relevant to the individual band only). The last four columns indicate respectively: (X) whether a parameter is natively computed by XMMN; (m) whether a parameter is available also in the band-merged table; (o) whether a parameter is present in the XLSSOPT table together with those described in Table 11; and (C) whether a parameter is present in the catalogue stored at CDS.

Column name	units	meaning and usage	X	m	o	C
Bseq or CDseq	–	internal sequence number (unique)		X	X	X
Bcatname or CDcatname	–	IAU catalogue name XLSSx Jhhmmss.s-ddmmss, x=B or CD		X	X	X
Xseq	–	pointer to merged entry see Table 10		X	X	X
Xcatname	–	pointer to merged entry see Table 10		X	X	X
Xfield	–	XMM pointing 1-32 for B01-B32 1001-1019 for G01-G19		X		
expm1	s	MOS1 camera exposure in the band	X			
expm2	s	MOS2 camera exposure in the band	X			
exppn	s	pn camera exposure in the band	X			
gapm1	"	MOS1 distance to nearest gap	X			
gapm2	"	MOS2 distance to nearest gap	X			
gappn	"	pn distance to nearest gap	X			
Bnearest or CDnearest	"	distance to nearest detected neighbour	X	X		
Bc1c2	0—1—2	1 for class C1, 2 for C2, 0 for undefined		X	X	X
CDc1c2	0—1—2	1 for class C1, 2 for C2, 0 for undefined				
Bcorerad or CDcorerad	"	core radius EXT (for extended sources)	X	X		X
Bextlike or CDextlike	–	extension likelihood EXT_LH	X	X		X
Bdetlik_pnt or CDdetlik_pnt	–	detection likelihood DET_LH for pointlike fit	X			
Bdetlik_ext or CDdetlik_ext	–	detection likelihood DET_LH for extended fit	X			
Boffaxis or CDoftaxis	'	off-axis angle		X		X
Brawra_pnt or CDrawra_pnt	degrees	source RA (not astrometrically corrected) for pointlike fit	X			
Brawdec_pnt or CDrawdec_pnt	degrees	source Dec (not astrometrically corrected) for pointlike fit	X			
Brawra_ext or CDrawra_ext	degrees	source RA (not astrometrically corrected) for extended fit	X			
Brawdec_ext or CDrawdec_ext	degrees	source Dec (not astrometrically corrected) for extended fit	X			
Bra_pnt or CDra_pnt	degrees	source RA (astrometrically corrected) for pointlike fit	X			
Bdec_pnt or CDdec_pnt	degrees	source Dec (astrometrically corrected) for pointlike fit	X			
Bra_ext or CDra_ext	degrees	source RA (astrometrically corrected) for extended fit	X			
Bdec_ext or CDdec_ext	degrees	source Dec (astrometrically corrected) for extended fit	X			
Bposerr or CDposerr	"	error on coordinates according to Table 6		X		X
Bratemos_pnt or CDratemos_pnt	cts/s	MOS count rate for pointlike fit	X			
Bratepn_pnt or CDratepn_pnt	cts/s	pn count rate for pointlike fit	X			
Bratemos_ext or CDratemos_ext	cts/s	MOS count rate for extended fit	X			
Bratepn_ext or CDratepn_ext	cts/s	pn count rate for extended fit	X			
countmos_pnt	cts	MOS number of counts for pointlike fit	X			
countpn_pnt	cts	pn number of counts for pointlike fit	X			
countmos_ext	cts	MOS number of counts for extended fit	X			
countpn_ext	cts	pn number of counts for extended fit	X			
bkgmos_pnt	cts/pixel	MOS local background for pointlike fit	X			
bkgpn_pnt	cts/pixel	pn local background for pointlike fit	X			
bkgmos_ext	cts/pixel	MOS local background for extended fit	X			
bkgpn_ext	cts/pixel	pn local background for extended fit	X			
Bflux or CDflux	erg/cm <sup>2</sup> /s	source flux (undefined i.e. -1 for extended)		X		X
Bfluxflag or CDfluxflag	0 to 2	0 if MOS-pn difference < 20%, 1 between 20%-50%, 2 above 50%		X		X

**Table 10.** List of database parameters, as Table 9, but for the additional columns present only in the merged catalogue table XLSS. When there are two column names given, one with the prefix B and one with the prefix CD, they relate to the given band, and both show up in the band-merged table. Column names with the prefix X are relevant to merged properties.

Column name	units	meaning and usage	X	m	o	C
Xseq	–	Internal sequence number (unique)		X	X	X
Xcatname	–	IAU catalogue name XLSS Jhhmmss.s-ddmmssc, see Sec. 2.3.7		X	X	X
Bspurious and CDspurious	0 or 1	set to 1 when soft/hard component has DET_LH < 15		X		
Bdetlike and CDdetlike	–	detection likelihood EXT_LH (pnt or ext according to source class)	X	X		X
Xra	degrees	source RA (astrometrically corrected) (pnt or ext according to source class and in best band)		X	X	X
Xdec	degrees	source Dec (astrometrically corrected) (pnt or ext according to source class and in best band)		X	X	X
Bra and CDra	degrees	source RA (astrometrically corrected) (pnt or ext according to source class)		X	X	X
Bdec and CDdec	degrees	source Dec (astrometrically corrected) (pnt or ext according to source class)		X	X	X
Xbestband	2 or 3	band with highest likelihood : 2 for B, 3 for CD		X		
Xastrocorr	1 or 2	astometric correction from CFHTLS (1) or USNO (2)		X		
Xmaxdist	"	distance between B and CD positions		X		
Xlink	–	pointer to Xseq of secondary association, see Sec. 2.3.7		X		
Bratemos and CDratemos	cts/s	MOS count rate (pnt or ext according to source class)	X	X		X
Bratepn and CDratepn	cts/s	pn count rate (pnt or ext according to source class)	X	X		X

**Table 11.** List of additional optical information presented as columns in the XLSSOPT table. The latter table also includes the X-ray columns marked as such in Tables 9 and 10. Therefore columns with the X, B or CD prefixes refer to X-ray parameters, those with the O prefix to optical data, and those without prefix to combined properties. The arrangement of CFHTLS W1 fields is given at <http://terapix.iap.fr/cplt/oldSite/Descart/cfhtls/cfhtlswidemosaiactargetW1.html>

Column name	units	meaning and usage	Terapix
Oseq	–	internal sequence number (unique)	n/a
Oid	–	original Terapix id in field	id
Ofield	–	CFHTS field identification in form $\pm x \pm y$	n/a see caption
Ora	degrees	RA of the optical candidate	ra
Odec	degrees	Declination of the optical candidate	dec
Oflag	–	binary flag combining 0/1 galaxy/star, 0/4 normal/masked, 0/8 normal/saturated	flag
Ou	magnitude	$u^*$ magnitude	u
Og	magnitude	$g'$ magnitude	g
Or	magnitude	$r'$ magnitude	r
Oi	magnitude	$i'$ magnitude	i
Oz	magnitude	$z'$ magnitude	z
Ou.e	magnitude	error on $u^*$ magnitude	uerr
Og.e	magnitude	error on $g'$ magnitude	gerr
Or.e	magnitude	error on $r'$ magnitude	rerr
Oi.e	magnitude	error on $i'$ magnitude	ierr
Oz.e	magnitude	error on $z'$ magnitude	zerr
distance	"	distance from the X-ray corrected position to the optical position	n/a
prob	–	chance probability of X-ray to optical association (see text)	n/a